

IET Renewable Power Generation

Special Issue Call for Papers

**Be Seen. Be Cited.
Submit your work to a new
IET special issue**

Connect with researchers and
experts in your field and
share knowledge.



Be part of the latest research
trends, faster.

[Read more](#)



The Institution of
Engineering and Technology

A simple method for estimating the effectiveness of reactive power-based low-voltage ride-through support of the distributed energy resources

Akbar Swandaru  | Mihai D. Rotaru | Jan K. Sykulski 

School of Electronics and Computer Science,
University of Southampton, Southampton, UK

Correspondence

Akbar Swandaru, School of Electronics and
Computer Science, University of Southampton,
Southampton, UK.
Email: as14g14@soton.ac.uk

Abstract

The increasing number of distributed energy resources (DERs) leads to the need for DER that can provide ancillary service, such as low-voltage ride-through (LVRT) voltage support. The support is made to improve the short-term voltage stability in power systems. Recently, DER LVRT voltage support through reactive power regulation are becoming common. Designing LVRT voltage support is highly influenced by the accuracy of the modelling and the data needed. However, in some cases, the required modelling can challenge the computational complexity, effort, and required data. Nevertheless, modelling the systems through an oversimplification may result in inaccuracies and hypothetical solution. Thus, the best compromise between model accuracy and simplicity will alleviate the problem. The study presents a methodology for estimating the effectiveness of the support. Unlike the commonly computer-assisted approach, such as the dynamic RMS simulation, the benefit of the methodology is on the computing process, which is much simpler since the dynamic DER modelling work is not needed, and the evaluation of the effectiveness can be achieved even when the grid information is incomplete. Its accuracy is validated against typical RMS simulation results obtained using PowerFactory Dlgilent software for well-characterised networks.

1 | INTRODUCTION

The implementation of distributed energy resources (DERs) has become a significant concern, especially when their extensive penetration is considered. It is well known that conventional power plants using synchronous generators can handle faults without the need to be disconnected while injecting short-circuit currents during a voltage dip. This feature of synchronous generators is crucial in a power system helping to raise the voltage around the location of the fault [1]. In the event under solid fault, the injection of the current will help to prevent the voltage level surrounding the faulted location from going down deeper, in an attempt to minimise the risk of further disturbance, such as blackout. Initially, DER's implementation and its impact related to the grid faults was not considered critical.

Hence, as a means of protecting the electronic components of the DERs, these inverter-based generating units were disconnected during grid faults. Such a disconnection mechanism can be achieved through under-voltage protection. However, with the increasing penetration of DERs, the disconnection may become counterproductive. Usually, when a grid fault occurs, the fault's impact can be sensed in a wide area surrounding the fault, as it propagates away from the fault site throughout the power system. Consequently, this can lead to several DER units automatically tripping. Such disconnection in series of DER groups will result in a considerable cascading loss of electricity generation. Therefore, to avoid the problems mentioned above, with the ongoing plans to increase the penetration of DER units, DER with reactive power support on low-voltage ride-through (LVRT) is necessary.

This is an open access article under the terms of the [Creative Commons Attribution](https://creativecommons.org/licenses/by/4.0/) License, which permits use, distribution and reproduction in any medium, provided the original work is properly cited.

© 2021 The Authors. *IET Renewable Power Generation* published by John Wiley & Sons Ltd on behalf of The Institution of Engineering and Technology

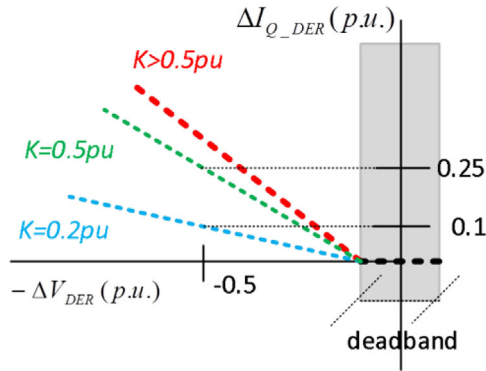


FIGURE 1 Reactive current support during low-voltage ride-through

1.1 | DER's LVRT voltage support

The DER's reactive power-based LVRT voltage support that is made through regulating the additional reactive current injection (aRCI) is a linear function of the voltage difference between the pre-fault condition and during the fault and of the injection level of the aRCI—known as the K -factor [2]. This implies that for any DER that experiences a voltage bus value outside a pre-specified dead band (Figure 1), a mitigating voltage control via aRCI (ΔI_{Q_DER}) regulation is required [3]. In other words, a deeper voltage drop during the fault necessitates a supply of more reactive current injection [4]; thus, if more reactive power support is available, the reduction in the voltage drop during the fault will be mitigated more effectively. The DER's LVRT reactive power support through regulating the aRCI is encouraged to become a standard in some of the renewable grid codes [5].

Furthermore, a DER with a conventional reactive power support capability can inject a reactive current up to the maximum rated value when the terminal voltage is in a sag while limiting the active current to zero. For this kind of reactive power support found in [6], it is argued that if the active power reference is set to zero during the sag, then all the available power could be dedicated to the reactive power support. The alternatives to reactive power injection (RPI) techniques include 'RPI with constant average active power control (RPI-Const-P)', 'RPI with constant active current control (RPI-Const- I_d)', and 'RPI with constant peak current control (RPI-Const- I_{g_max})' [7]. The objective of RPI-Const-P is to maximise the output energy using maximum power point tracking control during LVRT operation, whereas the average active power can be maintained constant in the short-term period of the fault. The RPI-Const- I_d offers flexibility to the injection given to the lower current rating inverters. The drawback of both RPI-Const-P and RPI-Const- I_d is, however, the possibility of overcurrent during LVRT. Hence, the RPI-Const- I_{g_max} was developed to prevent unintentional inverter shutdown due to overcurrent protection. The strategy is to allow the magnitude of the injected current to be kept constant but lower than the inverter current limitation during LVRT. While doing so, the active power will be reduced proportionally in order to inject sufficient reactive

power during LVRT. All three RPI strategies mentioned above require full reactive current to be injected in case of extreme voltage sag.

The influence of the DER's connection on the effectiveness of the ancillary support has been studied before. One particular conclusion was that on low-voltage-connected DERs, active power support via active current injection (aACI) is preferred over aRCI because LVRT voltage support through aACI tends to be more effective on a lower X/R ratio grid [8]. It was also shown in [8] through simulations that the doubly fed induction generator LVRT voltage support with reactive power control performs better in high X/R ratio systems. This argument seems aligned with [9], where it is argued that the parameters affect either the aRCI or aACI's effectiveness is the total impedance from the DER connection to the point of common coupling (PCC) and the X/R ratio of the total impedance to the PCC.

The DER's LVRT voltage support through a combination of active and reactive power support, via additional active and reactive current (aRACI), was considered in [10]. In particular, it is claimed in [10] that the impedance angle-adjusted aRACI leads to better effectiveness than either a pure aRCI or aACI. The higher effectiveness of the aACI was observed because the active and reactive currents, per the angle of the impedance between the DER and the located fault, could be kept within the active and reactive current transfer limits of the DER. The theory of the active and reactive current transfer limits of the DER may be found in [11]. In [10], however, it was argued that the impedance angle-adjusted aRACI was less effective in supporting the LVRT than a pure aRCI under reverse power flow situations.

It should be noted that many low-voltage-connected DERs, mainly photovoltaic (PV), are situated in housing estates. The PVs regularly reach their peak operation during daytime when the houses' loads are at their lowest. This implies that peak low-voltage-connected DERs will be mostly under a reverse power flow condition. Furthermore, an LVRT through aACI and aRACI needs a continuous standby of 'additional active reserve power' from the DER. Thus, the DER must be operated under a sub-optimum condition that is not economically favourable for long-term DER usage [12]. With this in mind, the aRACI—or even the aACI—should not be adopted as an LVRT support preference in future DER requirements.

Asymmetrical faults have also been an issue considered for DER LVRT voltage support [13]. It is argued that when a DER injects a pure positive-sequence aRCI during an asymmetrical fault, the positive-sequence grid voltage is improved, but unintentionally, the negative-sequence voltage increases too. This causes the voltages of the non-faulty phases to increase, which ultimately leads to overvoltage. The studies, as mentioned earlier, generally propose an improved reactive current injection mechanism, which is not only able to handle symmetrical faults but also asymmetrical faults. Even more, there have been recent studies reporting that inverter is now even capable of handling asymmetrical faults better [7]. This is indicating that DER is now becoming durable at handling asymmetrical disturbance.

However, currently, available grid requirements are still adopting positive-sequence-only reactive current injection, irrespective of the fault type. This is likely to remain in effect in the future, as it allows a more straightforward renewable grid planning. Consequently, in our study, we focus on symmetrical faults only.

All previous studies have concluded that the effectiveness of the DER's LVRT support (either aRCI, aACI, or aRACI) is influenced by the X/R ratio of the network. Through relevant simulations, it was shown that the DER's LVRT reactive power support (aRCI) is more effective in reducing the voltage drop during LVRT when the DER is connected to a higher X/R ratio, whereas for low-voltage-connected DERs, the reactive power support is less effective. While a complete simulation of the full network would allow the effectiveness of the reactive power support to be assessed, a simpler and faster analysis will assist the network operator in understanding and planning such support.

1.2 | Challenge on modelling

Evaluating the effectiveness of these LVRT voltage supports can be done through RMS simulation. However, with a detailed dynamic representation of a large number of DERs at distribution level in the simulation tool, it will increase the complexity of the models in terms of computational effort and data availability. On the other hand, modelling power systems elements through an oversimplification may result in a solution that does not represent well the problem that needs to be solved.

Defining the best compromise between model accuracy and simplicity on modelling power systems elements is not an easy task. As such, designing LVRT voltage support that will meet the desired needs, such as the magnitude, permitted duration of the lowest voltage sag and the balance/unbalance distribution matter, is highly influenced by the accuracy of the DER modelling of the corresponding grid and the required data availability [2, 14, 15].

When the decided LVRT voltage support is made, and obtaining the information regarding the criterion (minimum voltage sag that should be withstood, and the voltage sag improvement that should be made when necessary) is needed, one needs to build a simulation model including the DER models. Estimation of the effectiveness of the DER's LVRT voltage support through typical positive-sequence RMS simulation can be achieved when first, the required knowledge, and second, the data needed to construct the simulation blocks of the DER modelling, such as PV array, DC voltage controller, pulse-width modulation modelling, current controller, the diagram block of the LVRT voltage support, and so forth, are available [16]. When all previously mentioned information is available, the estimation is then done through the RMS simulation.

It can be inferred that a laborious task is needed for estimating the effectiveness of the DER's LVRT voltage support. Furthermore, often on many occasions, the information needed is incomplete, and hence the construction of the DER

modelling is done through approximations; still, extensive work and knowledge to construct the DER modelling are required.

Grid planner often poses problem relating to the grid data unavailability and challenges relating to the construction of the DER modelling [10]. A more straightforward approach to do the estimation may help the task at hand.

In this study, we propose a tool, based on a simple phasor analysis, to estimate the effectiveness of the DER's reactive power-based LVRT voltage support effectively without the need of the extensive work and the knowledge on DER modelling that is commonly necessary when using dynamic RMS simulation. The proposed methodology can estimate the effectiveness of the DER's LVRT voltage support, whereas its performance is commonly affected by the character of the DER connections, such as the X/R ratio of the network, and several other constraints that have not been investigated before, such as the increasing resultant steady-state voltage of the DER-connected bus, the potential value of the short-circuit impedance (Z_{SC}), the steady-state active and reactive power of the DER (P_{DER} and Q_{DER}), and the reactive power/aRCI $\Delta I_{reactive}/\Delta V$ level. The proposed methodology offers simplicity since it does not require the knowledge on constructing the DER modelling and thus could avoid problem relating to the DER data unavailability. Therefore, the main contribution of this study is a methodology and an approach to estimate the effectiveness of the LVRT voltage support that will benefit renewable grid planning.

2 | THE PROPOSED SIMPLE ANALYSIS METHOD

The basic principle behind the proposed approach is that the observed part of the network needs to be transformed using a simplified equivalent impedance description.

Consider a system with several nodes representing load points, for example, a housing complex, and its representation as shown in Figure 2. Each node denotes an aggregated loading point (at 220 V consumer-level voltage). The 'external network', outside the observed portion of the network, can be illustrated as an 'infinite node', which in this calculation serves as a 'voltage source'. Furthermore, suppose the planned location of the DER is at the most remote node ($n + 2$). Then, assuming the steady-state voltage profiles of all nodes are available through local measurements, the average peak and low active and reactive power consumptions (P_{avg_load} and Q_{avg_load}) may be profiled. Hence, the equivalent load impedance of each loading point (node), Z_{avg_load} , can be expressed as

$$Z_{avg_load} \angle \delta_{avg_load} = \frac{V_{load} \angle \delta_{load}^2}{(P_{avg_load} + jQ_{avg_load})^*} \quad (1)$$

where $V_{load} \angle \delta_{load}$ is obtained from the steady-state positive-sequence (phase-to-phase) voltage of the node. Assuming this analysis is for grid planning, $V_{load} \angle \delta_{load}$ can be easily obtained and is the steady-state nominal voltage before the DERs are

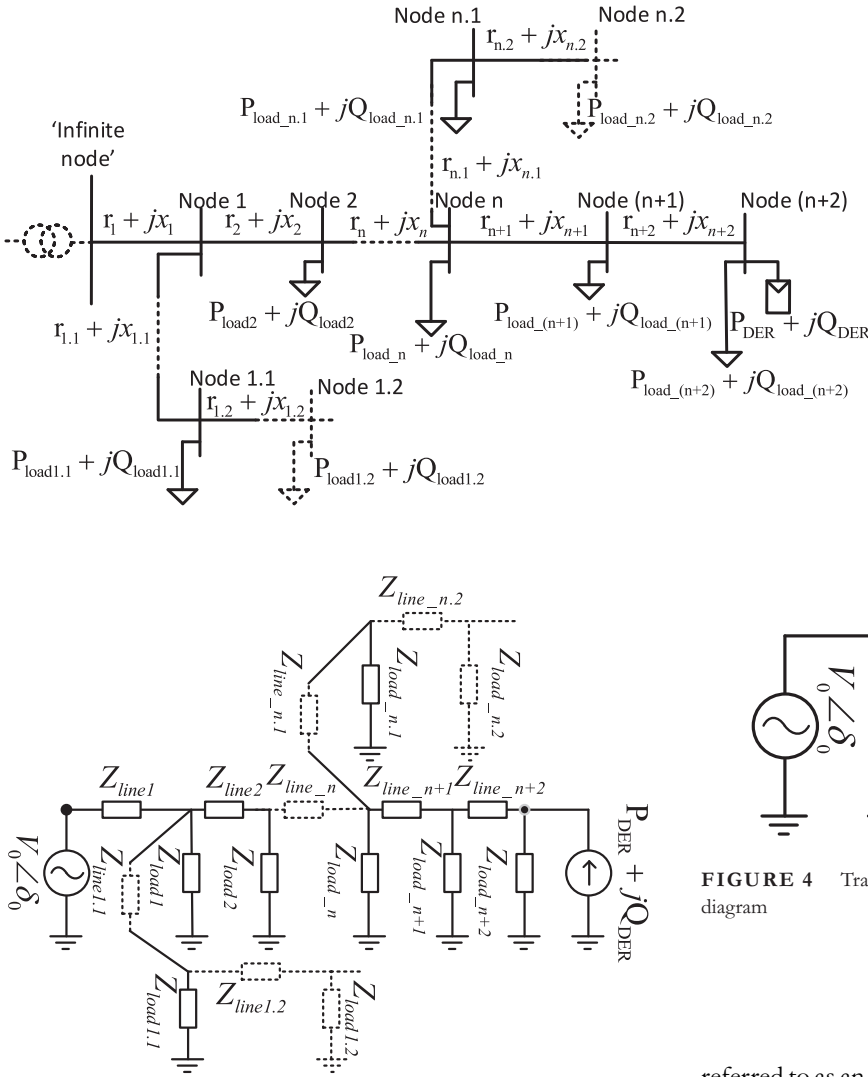


FIGURE 3 Transforming all active and reactive loads into impedances

implemented. The rising steady-state nominal voltage due to the presence of the DER will be considered in the third step.

The aggregated DERs are represented as current sources. Figure 3 shows the impedance representation of the loads along with the DERs as current sources, which can now be used for the second step of establishing the equivalent Thevenin circuit.

To obtain the equivalent Thevenin circuit representation of the network, several stars to delta transformations (Y to Δ) may be necessary. These transformations are generalised into Figure 4.

$Z_{inf_node_th}$, Z_{line_th} , and Z_{load_th} are obtained through Y to Δ transformations. However, it should be noted that $Z_{ext_grid} \gg Z_{inf_node_th}$, as Z_{ext_grid} is the overall impedance of the external part of the observed network. Therefore, the impedance at the infinite bus of the equivalent Thevenin circuit ($Z_{inf_node_th}$) should be represented by Z_{ext_grid} . This is shown in the later equivalent Thevenin circuit representation in Figure 5.

In essence, the external grid represents an 'external element' that is outside of the system under consideration (this can be

FIGURE 2 An example distribution part of a network

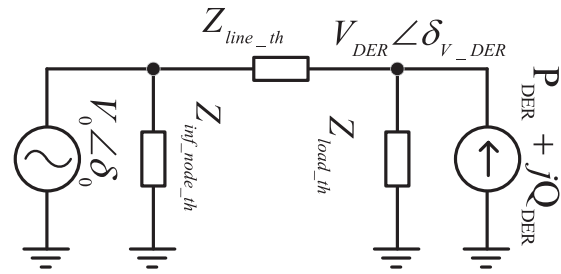


FIGURE 4 Transforming the circuit of Figure 3 into a simplified Thevenin diagram

referred to as an element outside the HV side of the transformer that is connected to the 'infinite node' in Figure 2). However, for the sake of the analysis, one should define it as an existing element in the form of aggregated properties that affect the calculations [17]. These properties include the short-circuit current I_k'' , the positive-sequence nominal voltage $V_0 \angle \delta_0$ and its positive-sequence X/R ratio of the 'external grid' [18]. Technically I_k'' is the value of the short-circuit current at the feeder connection point, which in this sense is the 'infinite node' in Figure 2. Thus, if I_k'' is known, the equivalent impedance Z_{ext_grid} of the external grid at the 'infinite node' is given by

$$Z_{ext_grid} = \frac{c_{factor} \cdot U_{ext_grid}}{\sqrt{3} \cdot I_k''} \quad (2)$$

where c_{factor} represents a voltage correction factor for the measured positive-sequence voltage at the external grid [17]. If the X/R ratio is known as well, then R_{ext_grid} and X_{ext_grid} can be estimated as

$$X_{ext_grid} = \frac{Z_{ext_grid}}{\sqrt{1 + \left(\frac{X}{R}\right)^{-2}}} \quad (3)$$

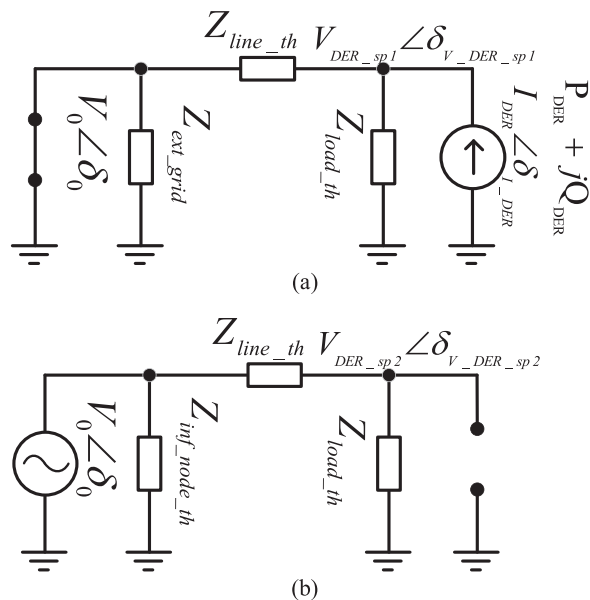


FIGURE 5 Superposition using the simplified Thevenin circuit from the second step (a) using external grid as a source, and (b) using distributed energy resource as a source

$$R_{ext_grid} = \left(\frac{X}{R}\right)^{-1} \cdot X_{ext_grid} \quad (4)$$

In the absence of national standards, it seems reasonable to choose a voltage correction factor between 0.95 and 1.10 [17]. However, for simplicity, the value of one has been assumed. Z_{ext_grid} is used to represent the ‘characteristic’ of the external grid. If the intention is to estimate I''_k , for example, through the well-known short-circuit numerical analysis [17], this can be done by isolating the observed grid from the node where the HV transformer is feeding to, and then perform a short-circuit calculation. Then, one can obtain I''_k , the short-circuits R and X , to establish the X/R ratio. Alternatively, these properties can be found from the grid data [18]. $V_0 \angle \delta_0$ is obtained from the low-voltage side of the transformer in Figure 2. For simplicity, $V_0 \angle \delta_0$ is taken as a reference, and thus δ_0 is set as zero.

The Thevenin circuit derived is crucial since it is used to estimate the increased steady-state voltage due to the DER’s presence ($V_{DER} \angle \delta_{V_DER}$), which is the third step in our methodology. From this, the resultant of the aRCI (ΔI_{Q_DER} , later on) is determined in step four. $V_{DER} \angle \delta_{DER}$ is obtained by using the ‘usual’ superposition analysis, which is later modified with the available parameters. The purpose of the modification is explained later.

To estimate the increased steady-state load bus voltage due to the DER connection ($\Delta V_{DER} \angle \Delta \delta_{V_DER}$), first, the simplified Thevenin circuit diagram in Figure 4 that was used for our superposition analysis is transformed into two points of reference as shown in Figures 5 (a) and (b). The first reference (Figure 5(a)) considers the external grid voltage source as

a short circuit, while the second reference (Figure 5(b)) treats the DER as an open source. Note that to do the superposition analysis, the DER is commonly represented as a current source. This is shown in the first reference (Figure 5(a)). Assuming that for grid planning the rated active and reactive power of the DERs of $P_{DER} + jQ_{DER}$ is obtained, it would be impossible to obtain $I_{DER} \angle \delta_{I_DER}$ without knowing the nominal voltage at the load node that is already connected with the DERs ($V_{DER} \angle \delta_{V_DER}$), which in fact is the aim of the calculation. Therefore, to obtain $V_{DER} \angle \delta_{V_DER}$, a modification of the calculation is necessary. This can be accomplished by assuming the DER element to be a negative load or defining the DER’s element as ‘negative impedance’.

Treating the DER element as a negative load or negative impedance is a common approach [19] and is usually used for small, distributed power source in a grid. The term negative load was made because of its presentation, and it is often attributed as ‘negative load’ since it provides the source. This normally can be referred to as a rooftop PV. Treating the DER’s element in a network modelling of a study as ‘negative load’ is a common way for steady-state voltage rise calculations due to DER’s presence. However, this approach is not as accurate as when the DER is defined as a ZIP model [20]. Nevertheless, defining the DER element as a negative load is still acceptable for the purpose of steady-state voltage rise estimation for relatively more uncomplicated systems. The network simplification made in the second step is used here again.

First, the condition when the DER is present while the grid reference node is assumed to have zero voltage (Figure 5(a)) is considered. Under this condition, the steady-state voltage at the Thevenin load node $V_{DER_sp1} \angle \delta_{DER_sp1}$ may be found as

$$V_{DER_sp1} \angle \delta_{DER_sp1} = (I_{DER} \angle \delta_{I_DER}) \cdot \frac{Z_{load_th} \cdot Z_{line_th}}{Z_{load_th} + Z_{line_th}} \quad (5)$$

In the second case, the grid reference node is considered while the DER is assumed to have zero current (open circuit) (Figure 5(b)). Therefore, the steady-state voltage at the Thevenin load node $\Delta V_{DER_sp2} \angle \Delta \delta_{DER_sp2}$ may be obtained from

$$V_{DER_sp2} \angle \delta_{DER_sp2} = (V_0 \angle \delta_0) \cdot \frac{Z_{load_th}}{Z_{load_th} + Z_{line_th}} \quad (6)$$

The actual increased steady-state voltage $V_{DER} \angle \delta_{DER}$ is then obtained by combining Equations (5) and (6)

$$V_{DER} \angle \delta_{V_DER} = \left(V_{DER_sp1} \angle \delta_{DER_sp1} \right) + \left(V_{DER_sp2} \angle \delta_{DER_sp2} \right) \quad (7)$$

Upon grid DER planning, if the DER’s capacity plan is defined with active and reactive power ($P_{DER} + jQ_{DER}$), then $V_{DER_sp1} \angle \delta_{DER_sp1}$ in Equation (5) cannot be obtained, as to find $I_{DER} \angle \delta_{I_DER}$, the value of the increased voltage $V_{DER} \angle \delta_{V_DER}$ is needed. Therefore, as an alternative,

from $P_{DER} + jQ_{DER}$, one could treat it as a negative load $-(P_{DER} + jQ_{DER})$. Then, the $Z_{load_th} \angle \theta_{load_th}$ is modified into $Z_{loadDER_th} \angle \theta_{loadDER_th}$

$$Z_{loadDER_th} \angle \theta_{loadDER_th} = \frac{V_{load} \angle \delta_{V_load}^2}{(P_{load_th} - P_{DER} + jQ_{load_th} - jQ_{DER})^*} \quad (8)$$

Here, $V_{load} \angle \delta_{V_load}$ is the steady-state voltage of the load node without the DER connections. This can be easily obtained through local voltage measurement upon grid planning.

Note that in the second step, the equivalent load is still represented by $Z_{load_th} \angle \theta_{load_th}$. Then, $Z_{load_th} \angle \theta_{load_th}$ is transformed in Equation (8) into a form of $P_{load_th} + jQ_{load_th}$ by simply using Equation (1). After $P_{load_th} + jQ_{load_th}$ is found, Equation (8) is substituted to Equation (6). $\frac{Z_{load_th}}{Z_{load_th} + Z_{line_th}}$ in Equation (6) describes the overall impedance that represents both the load and the DER element. This modification yields the actual increased steady-state voltage.

$$V_{DER} \angle \delta_{V_DER} = (V_0 \angle \delta_0) \cdot \frac{Z_{loadDER_th} \angle \theta_{loadDER_th}}{Z_{loadDER_th} \angle \theta_{loadDER_th} + Z_{line_th}} \quad (9)$$

The steady-state voltage rise due to the DER connection could then be estimated using the above equation. The results from this approach are validated by simulations using PowerFactory Digsilent, as reported in Section 3, as in results of $V_{DER} \angle \delta_{V_DER}$ from Table 2.

With $V_{DER} \angle \delta_{V_DER}$ now calculated, the fourth step can be undertaken. This step estimates the potential voltage sag at the DER's connection node ($V_{DER_f} \angle \delta_{V_DER_f}$). As mentioned in the introduction, a phase transmission line fault is used as an illustration. Suppose a transmission fault occurs somewhere in the outside part of the observed network and causes a voltage sag at the 'infinite node' in Figure 2. This will cause the voltage at the 'infinite node' to sag. The fault estimation can be done using a conventional symmetrical component fault analysis. The fault impedance Z_f includes the effect of the transmission line on the voltage drop at the observation point (represented as $V_0 \angle \delta_0 - \Delta V_f \angle \Delta \delta_{V_f}$ in Figure 6). The fault is shown as a red dot in Figure 6. Note that since a phase fault is used to illustrate the method, the observed system representation is given for the positive sequence only. In Figure 6, $I_f \angle \delta_{I_f}$ represents the short-circuit current contribution from ($V_0 \angle \delta_0 - \Delta V_f \angle \Delta \delta_{V_f}$), $I_{line_th_f} \angle \delta_{I_line_th_f}$ represents the short-circuit current contributed from the line, $I_{load_th_f} \angle \delta_{I_load_th_f}$ is the short-circuit current contributed from the load while $I_{DER_f} \angle \delta_{I_DER_f}$ is the short-circuit current contributed from the DER.

Before estimating $V_{DER_f} \angle \delta_{V_DER_f}$, the knowledge of $I_{line_th_f} \angle \delta_{I_line_th_f}$ is required. However, the short-circuit current $I_f \angle \delta_{I_f}$ is needed in order to get $I_{line_th_f} \angle \delta_{I_line_th_f}$. It

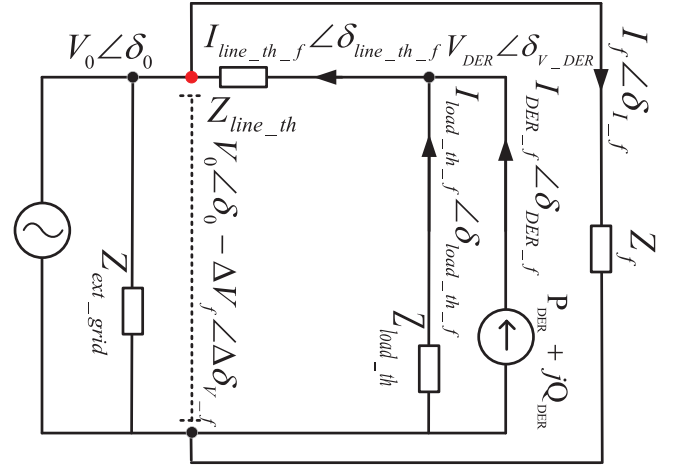


FIGURE 6 Representation of the observed system under fault condition

can be seen from Figure 6 that $I_f \angle \delta_{I_f}$ could be obtained from

$$I_f \angle \delta_{I_f} = \frac{V_0 \angle \delta_0}{Z_{3ph_th} + Z_f} \cdot \frac{1}{\sqrt{3}} \quad (10)$$

with

$$Z_{3ph_th} = (Z_{line_th} + Z_{loadDER_th}) // Z_{ext_grid} \quad (11)$$

Note that $Z_{loadDER_th}$ is obtained from Equation (8) as previously explained. Then, by using the same Figure 6, $I_{line_th_f} \angle \delta_{I_line_th_f}$ can be found as

$$I_{line_th_f} \angle \delta_{I_line_th_f} = \frac{Z_{ext_grid}}{Z_{ext_grid} + Z_{line_th} + Z_{loadDER_th}} \cdot I_f \angle \delta_{I_f} \quad (12)$$

Once $I_{line_th_f} \angle \delta_{I_line_th_f}$ is obtained, then $V_{DER_f} \angle \delta_{V_DER_f}$ may be estimated by first calculating $\Delta V_{DER_f} \angle \Delta \delta_{V_DER_f}$

$$\Delta V_{DER_f} \angle \Delta \delta_{V_DER_f} = \sqrt{3} \cdot Z_{loadDER_th} \cdot I_{line_th_f} \angle \delta_{I_line_th_f} \quad (13)$$

and then finding $V_{DER_f} \angle \delta_{V_DER_f}$ as

$$V_{DER_f} \angle \delta_{V_DER_f} = V_{DER} \angle \delta_{V_DER} - \Delta V_{DER_f} \angle \Delta \delta_{V_DER_f} \quad (14)$$

Note that $V_{DER} \angle \delta_{V_DER}$ was obtained in the third step (see Equation 9).

After $V_{DER_f} \angle \delta_{V_DER_f}$ has been estimated, the fifth step of the proposed methodology may be triggered. The magnitude of the aRCI (ΔI_{Q_DER}) can be estimated. The aRCI during the

LVRT, ΔI_{Q_DER} is defined as

$$\Delta I_{Q_DER} = K_{I_q} \cdot \frac{\left| \Delta V_{DER_f} \angle \Delta \delta_{V_DER_f} \right| \mp V_{db}}{V_0 \angle \delta_0} \quad (15)$$

where K_{I_q} is the K -factor as explained in Figure 1 [10]. The DER's reactive current I_{Q_DER} during LVRT is described by

$$I_{Q_DER} = I_{q_ref} = \begin{cases} I_{Q_DER_prefault} + \Delta I_{Q_DER}, & -I_{max} \leq I_{Q_DER} \\ \leq I_{max}, & -I_{max} > I_{Q_DER} > I_{max} \end{cases} \quad (16)$$

where $I_{Q_DER_prefault}$ is the DER's pre-fault reactive current that is simply obtained from

$$I_{Q_DER_prefault} = I_{DER_prefault} \cdot \cos(\varphi) \quad (17)$$

where φ is

$$\varphi = \tan^{-1} \left(\frac{\text{imaginary}(S_{DER}^*)}{\text{real}(S_{DER}^*)} \right) + \delta_{V_DER_f} \quad (18)$$

while $I_{DER_prefault}$ is the DER's pre-fault current

$$I_{DER_prefault} = \frac{S_{DER}}{\sqrt{3} \cdot (V_{DER} \angle \delta_{V_DER})^*} \quad (19)$$

Here, $\mp V_{db}$ (Equation 15) represents the voltage dead-band in per unit as illustrated in Figure 1. However, our investigation is concerned about providing the means of evaluating the effectiveness of the aRCI. Adding voltage dead-band into consideration would not signify the purpose of the study (not the primary constraint that shall give direct effect to the voltage support performance). For simplicity, the voltage dead-band is omitted. When the DER is injecting reactive current, the active current I_{P_DER} during LVRT is given by

$$I_{P_DER} = I_{d_ref} = I_{max} - \left| I_{Q_DER} \right| \quad (20)$$

This is to prevent the DER's inverter to be at risk of overcurrent and, thus, overheating due to this reactive control strategy [2]. In Equation (20), $I_{max} = 1$. Hence, the DER current during LVRT $I_{DER_f} \angle \delta_{I_DER_f}$ can be defined as

$$I_{DER} \angle \delta_{I_DER} = I_{P_DER} + j I_{Q_DER} \quad (21)$$

However, note that $I_{P_DER} + j I_{Q_DER}$ in Equations (15) to (21) is defined on the stationary reference frame. To use the grid synchronous reference frame, $I_{P_DER} + j I_{Q_DER}$ has to be synchronised with the grid frequency. This is done [21] by converting Equation (21) into

$$I_{DER} \angle \delta_{I_DER} = (I_{d_ref} \cdot \cos \theta' - I_{q_ref} \cdot \sin \theta')$$

$$+ j (I_{d_ref} \cdot \sin \theta' + I_{q_ref} \cdot \cos \theta') \quad (22)$$

where $\cos \theta'$ and $\sin \theta'$ relate to the dq/stationary reference frame of the DER. In practice, this procedure can be done by the phase-locked loop (PLL) device of the DER's inverter. In our method, $\cos \theta'$ and $\sin \theta'$ are represented as

$$\cos \theta' = \frac{\text{real}(V_{DER_f} \angle \delta_{V_DER_f})}{\text{absolute}(V_{DER_f} \angle \delta_{V_DER_f})} \quad (23)$$

$$\sin \theta' = \frac{\text{imaginary}(V_{DER_f} \angle \delta_{V_DER_f})}{\text{absolute}(V_{DER_f} \angle \delta_{V_DER_f})} \quad (24)$$

Note that the real and imaginary parts of $I_{DER} \angle \delta_{I_DER}$ in Equation (22) are the orthogonal axes of the synchronous reference frame. Thus, I_{Q_DER} in Equation (19) may be defined as the q-axis current reference of the DER (I_{q_ref}), whereas I_{P_DER} in Equation (20) as the d-axis current reference (I_{d_ref}). In this method, $I_{DER} \angle \delta_{I_DER}$ in Equations (21) and (22) applies to a fault condition as well; hence,

$$I_{DER_f} \angle \delta_{I_DER_f} = I_{DER} \angle \delta_{I_DER} \quad (25)$$

Equation (25) is essential, as with $I_{DER} \angle \delta_{I_DER}$, it allows the effectiveness of the aRCI to be evaluated. This can be done by performing the procedures from Equations (15) to (25) twice, first, by applying the DER's K -factor $K_{I_q} = 0$, and then applying DER's K -factor K_{I_q} with the desired setup. After two different values of $I_{DER} \angle \delta_{I_DER}$ have been obtained, say $(I_{DER_f} \angle \delta_{I_DER_f})_{K_{I_q}=0}$ and $(I_{DER_f} \angle \delta_{I_DER_f})_{K_{I_q}=n}$, then $\Delta I_{DER_f} \angle \Delta \delta_{I_DER_f}$ can be calculated as follows.

$$\Delta I_{DER_f} \angle \Delta \delta_{I_DER_f} = (I_{DER_f} \angle \delta_{I_DER_f})_{K_{I_q}=n} - (I_{DER_f} \angle \delta_{I_DER_f})_{K_{I_q}=0} \quad (26)$$

Here, $\Delta I_{DER_f} \angle \Delta \delta_{I_DER_f}$ represents the difference of DER's current contributions during a fault condition with and without the aRCI. Therefore, by adding $\Delta I_{DER_f} \angle \Delta \delta_{I_DER_f}$ with $I_f \angle \delta_{I_f}$ from Equation (10), the short-circuit current of the system with aRCI-enabled DER, $I_{f_aRCI} \angle \delta_{I_f_aRCI}$ can be estimated as

$$I_{f_aRCI} \angle \delta_{I_f_aRCI} = I_f \angle \delta_{I_f} + \Delta I_{DER_f} \angle \Delta \delta_{I_DER_f} \quad (27)$$

After $I_{f_aRCI} \angle \delta_{I_f_aRCI}$ has been found, Equations (12) to (14) are repeated with $I_f \angle \delta_{I_f}$ from Equation (12), replaced by $I_{f_aRCI} \angle \delta_{I_f_aRCI}$. The improved voltage due to DER's aRCI is given as $V_{DER_f} \angle \delta_{V_DER_f}$ from Equation (14). $(V_{DER_f} \angle \delta_{V_DER_f})_{K_{I_q}=n}$ is the improved voltage sag, while $(V_{DER_f} \angle \delta_{V_DER_f})_{K_{I_q}=0}$ is the non-improved voltage sag. Finally, the effectiveness of the DER's aRCI could be evalu-

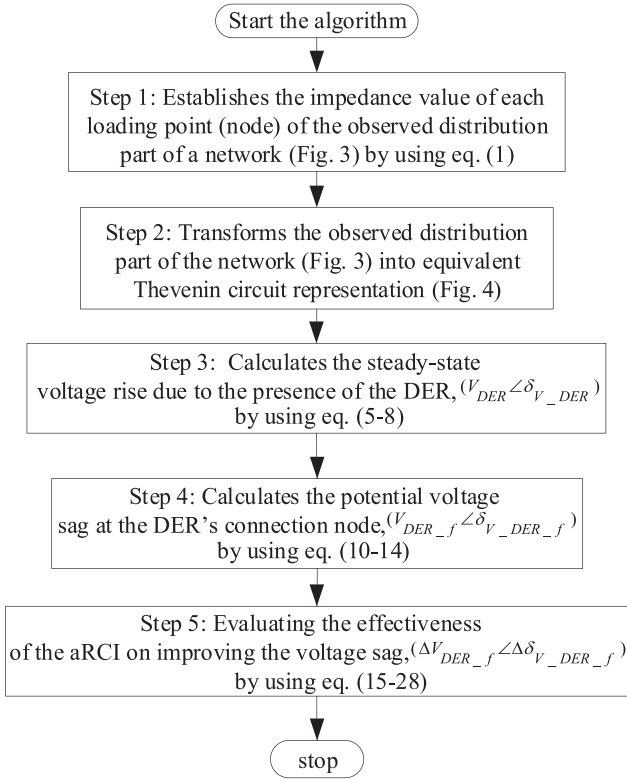


FIGURE 7 Overall flowchart of the proposed methodology

ated by comparing the different voltage sags between the cases with and without aRCI, namely, $(V_{DER_f} \angle \delta_{V_DER_f})_{K_{Iq}=n}$ and $(V_{DER_f} \angle \delta_{V_DER_f})_{K_{Iq}=0}$ as

$$\Delta V_{DER_f} \angle \Delta \delta_{V_{DER_f}} = (V_{DER_f} \angle \delta_{V_{DER_f}})_{K_{Iq}=n} - (V_{DER_f} \angle \delta_{V_{DER_f}})_{K_{Iq}=0} \quad (28)$$

The flowchart of the proposed methodology is depicted in Figure 7.

3 | VERIFICATION OF THE PROPOSED METHODOLOGY

In order to validate the proposed methodology, a typical low-voltage distribution network is assumed. Regular distribution networks have a low X/R ratio (systems below 35 kV usually have the X/R ratio of 10 or less, IEC-60909). In other word, low-voltage distribution network can be assumed to have such characteristic. Therefore, the network used for the purpose of this evaluation has similar characteristics. The effectiveness of the aRCI with respect to low X/R ratio can be assessed by studying different possible low X/R ratio values.

The simplified Thevenin Circuit Diagram of the test network is shown in Figure 4, whereas the parameters assumed for the estimation are shown in Table 1. Five samples of the case are

TABLE 1 The observed system parameters in Thevenin circuit diagram

Parameters	$R_{line_th} + jX_{line_th}$ (pu)	$V_{load} \angle \delta_{V_load}$ (pu \angle deg)
case 1	0.0072 + j. 0.0072	0.987 \angle -0.75
case 2	0.0072 + j. 0.0216	0.9879 \angle -2.21
case 3	0.0072 + j. 0.036	0.9875 \angle -3.68
case 4	0.0072 + j. 0.0505	0.9864 \angle -5.15
case 5	0.0072 + j. 0.0649	0.9846 \angle -6.63

TABLE 2 Comparison of steady-state voltage rise result between the proposed and the Powerfactory DIgsilent methods

Results	$V_{DER} \angle \delta_{V_DER}$ (pu \angle deg)	
Method used	DIgsilent	Proposed method
case 1	0.998 \angle -0.18	0.998 \angle -0.15
case 2	0.999 \angle -0.47	0.998 \angle -0.45
case 3	1.000 \angle -0.77	0.999 \angle -0.75
case 4	1.001 \angle -1.07	1.000 \angle -1.04
case 5	1.001 \angle -1.36	1.003 \angle -1.33

chosen. The MVA_{base} is chosen as 5MVA.

Assuming the short-circuit apparent power, S''_k , for all cases to be 20 MVA, yields the per-unit value of 4 pu. Distribution load power at the Thevenin bus, P_{load_th} (pu), is one pu. The validation case uses 80% DER penetration; hence, MVA_{DER} is set to 0.8 pu. The fault impedance Z_f is set to $0.144 + j0.144$ pu for all cases. The load node voltage is assumed to be already known through regular checks. Each case for the system has different equivalent line impedance, $R_{line_th} + jX_{line_th}$, as shown in Table 1. X/R ratio of the external grid, $R_{ext_grid} + jX_{ext_grid}$, are chosen uniformly $0.01436 + j0.1436$ per unit.

3.1 | Steady-state voltage rise results analysis

The results estimated using the proposed methodology have been compared with the same results obtained using the DIgsilent as shown in Table 2. The estimation difference of the proposed methodology as compared to the results obtained using the DIgsilent are shown in Table 3.

It can be seen that the steady-state voltage rise, V_{DER} , are estimated quite accurately by the proposed method. For V_{DER} , as shown in Table 2, a reasonably small estimation difference is observed for all cases. For instance, the V_{DER} estimation obtained using the proposed method for case 1 has an estima-

TABLE 3 % | Estimation difference | of steady-state voltage rise result between the proposed and the Powerfactory DIgsilent methods

Results	Case 1	Case 2	Case 3	Case 4	Case 5
$ V_{DER} $	0.037	0.078	0.067	0.003	0.123
δ_{V_DER}	14.544	5.0697	3.107	2.468	2.327

TABLE 4 Comparison of non-additional reactive current injection (aRCI)-enabled low-voltage ride-through (LVRT) voltage control results ('no voltage support' case) between the proposed method and the Powerfactory Digsilent simulations

Results	Method used	Case 1	Case 2	Case 3	Case 4	Case 5
$V_{DER_f} \angle \delta_{V_DER_f}$ (pu/deg)	Digsilent	0.610 \angle -9.87	0.609 \angle -9.47	0.608 \angle -9.07	0.609 \angle -8.67	0.609 \angle -8.28
	Proposed method	0.620 \angle -7.34	0.620 \angle -6.64	0.620 \angle -5.95	0.622 \angle -5.29	0.625 \angle -4.65
$I_{dq_absolute_f}$ (pu)	Digsilent	1.000	1.000	1.000	1.000	1.000
	Proposed method	0.997	0.992	0.987	0.982	0.977
$I_{d_ref_f}$ (pu)	Digsilent	1.000	1.000	1.000	1.000	1.000
	Proposed method	0.997	0.992	0.987	0.982	0.977
$I_{q_ref_f}$ (pu)	Digsilent	0.004	0.009	0.014	0.019	0.024
	Proposed method	0.003	0.008	0.013	0.018	0.023
$I_{P_DER_f}$ (pu)	Digsilent	0.986	0.988	0.990	0.991	0.993
	Proposed method	0.990	0.986	0.983	0.979	0.976
$I_{Q_DER_f}$ (pu)	Digsilent	-0.168	-0.156	-0.144	-0.132	-0.12
	Proposed method	-0.125	-0.107	-0.089	-0.072	-0.056

TABLE 5 % |Estimation difference| of non-aRCI-enabled LVRT voltage control result ('no voltage support' case)

Results	V_{DER_f}	$\delta_{V_DER_f}$	$I_{dq_absolute_f}$	$I_{d_ref_f}$	$I_{q_ref_f}$	$I_{P_DER_f}$	$I_{Q_DER_f}$
Case 1	1.675	25.584	0.260	0.260	25.714	0.375	25.610
Case 2	1.773	29.882	0.780	0.790	7.059	0.132	31.498
Case 3	2.023	34.386	1.300	1.290	3.704	0.657	38.046
Case 4	2.167	39.063	1.800	1.800	2.151	1.201	45.317
Case 5	2.578	43.836	2.290	2.291	2.521	1.733	53.333

tion difference for 0.037% for $|V_{DER}|$. The most substantial estimation difference rate for $|V_{DER}|$ is to be found for case 5, which is 0.123% and is still acceptably small. Although estimation difference for δ_{V_DER} for case 1 is 14.544%, which is comparatively more extensive than the remaining cases, the proposed method that has an angle at -0.15 degree, which is comparable with the Digsilent method that has δ_{V_DER} at -0.18 .

3.2 | 'LVRT with no voltage support' case results (scenario 1)

The comparison of non-aRCI-enabled LVRT result ('no voltage support' case) between the proposed and the PowerFactory Digsilent methods are shown in Table 4. For V_{DER_f} , the largest estimation difference is observed for case 5 (2.578%), whereas the smallest estimation difference is observed for case 1 (1.675%). The remaining estimation difference between the two methods is shown in Table 5. $I_{dq_absolute_f}$ represents the current magnitude in per unit, $I_{d_ref_f}$ represents the current magnitude in per unit in d axial of the dq axis in per unit, $I_{q_ref_f}$ represents the current magnitude in per unit in q axial of the dq axis in per unit, $I_{P_DER_f}$ represents the active current magnitude in per unit, and $I_{Q_DER_f}$ represents the reactive current magnitude in per unit.

It can be seen the estimation difference between the proposed and the Powerfactory Digsilent methods, particularly on voltage sag magnitude, V_{DER_f} , are acceptably small. According to Wu et al. [22], on a voltage magnitude estimations, estimating estimation differences of around 3% are acceptable.

3.3 | 'LVRT with voltage support via aRCI on K-factor = 0.5' case results (scenario 2)

The scenario on LVRT voltage support via aRCI with K -factor 0.5 is presented. The comparison of aRCI-enabled LVRT result between the proposed and the Powerfactory Digsilent methods are shown in Table 6. It can be seen from the table that the voltage sag V_{DER_f} improvement is observed as compared with the 'non-aRCI' case as shown previously in Table 4. For instance, in case 1, the voltage sag for 'non-aRCI' case, as shown in Table 4, are estimated 0.610 and 0.620 pu through Digsilent and the proposed methods, respectively. The voltage sag for 'aRCI with K -factor = 0.5' case is estimated as 0.623 pu (Digsilent method) and 0.634 pu (proposed method). Therefore, with aRCI, one could conclude that LVRT voltage support may improve voltage sag during the fault. The voltage sag improvement is observed 1.280% and 1.345% according to the Digsilent and the proposed method, respectively,

TABLE 6 Comparison of aRCI-enabled LVRT voltage control result (with voltage support case) between the proposed and the Powerfactory DIgsilent methods $K = 0.5$

Results	Method used	Case 1	Case 2	Case 3	Case 4	Case 5
$V_{DER_f} \angle \delta_{V_DER_f}$ ($p\mu/\angle deg$)	DIgsilent	0.623 \angle -12.76	0.625 \angle -12.71	0.627 \angle -12.65	0.629 \angle -12.61	0.631 \angle -12.57
	Proposed method	0.634 \angle -5.99	0.642 \angle -5.42	0.642 \angle -4.86	0.644 \angle -4.32	0.646 \angle -3.81
$I_{dq_absolute_f}$ ($p\mu$)	DIgsilent	0.834	0.834	0.835	0.835	0.835
	Proposed method	0.831	0.827	0.823	0.819	0.816
$I_{d_ref_f}$ ($p\mu$)	DIgsilent	0.812	0.812	0.811	0.810	0.810
	Proposed method	0.809	0.803	0.798	0.792	0.788
$I_{q_ref_f}$ ($p\mu$)	DIgsilent	0.190	0.194	0.198	0.201	0.205
	Proposed method	0.191	0.197	0.202	0.207	0.212
$I_{P_DER_f}$ ($p\mu$)	DIgsilent	0.834	0.834	0.835	0.834	0.835
	Proposed method	0.827	0.820	0.814	0.808	0.802
$I_{Q_DER_f}$ ($p\mu$)	DIgsilent	0.006	0.011	0.015	0.019	0.024
	Proposed method	0.086	0.103	0.119	0.134	0.148

TABLE 7 % |Estimation difference| of aRCI-enabled LVRT voltage control result with $K = 0.5$ (with voltage support)

Results	V_{DER_f}	$\delta_{V_DER_f}$	$I_{dq_absolute_f}$	$I_{d_ref_f}$	$I_{q_ref_f}$	$I_{P_DER_f}$	$I_{Q_DER_f}$
Case 1	1.823	53.029	0.348	0.419	0.632	0.899	93.039
Case 2	2.704	57.335	0.863	1.047	1.651	1.631	89.689
Case 3	2.505	61.594	1.402	1.64	2.481	2.421	87.352
Case 4	2.398	65.742	1.892	2.209	3.182	3.082	85.479
Case 5	2.488	69.722	2.334	2.716	3.564	3.904	84.011

whereas on case with highest X/R ratio of the system, case 5, the voltage sag improvement is observed 2.15% (DIgsilent method) and 2.12% (proposed method), respectively. The overall voltage sag improvement of the aRCI-enabled system between the proposed and the DIgsilent methods in percentage (with K -factor = 0.5) are presented in Table 10 in the column ‘comparison A’.

In Table 7, the difference of aRCI-enabled LVRT result with K -factor = 0.5 between the proposed and the Powerfactory DIgsilent methods is presented. It can be seen the estimation difference between the proposed and the Powerfactory DIgsilent methods, particularly on voltage sag magnitude V_{DER_f} , are reasonably acceptable.

3.4 | ‘LVRT with maximum aRCI’ case results (scenario 3)

The scenario on LVRT voltage support via maximum aRCI is presented. To create maximum aRCI, K -factor is set arbitrarily as six. The comparison for aRCI-enabled LVRT results are shown in Table 8. It can be seen from the table that better voltage sag V_{DER_f} improvements are observed as compared in scenario 2. These voltage sag reductions can be seen as improvements due to the higher K -factor.

Both methodologies, DIgsilent and the proposed approach, show improvements in terms of voltage sag for aRCI cases when compared with the ‘non-aRCI’ cases. The improvements are more substantial for the test cases that have higher X/R ratios. The overall voltage sag improvement of the maximum aRCI-enabled system calculated with the proposed and the DIgsilent methods in percentage are presented in Table 9. It can be seen the resulting estimation difference of voltage sag magnitude V_{DER_f} on the proposed method are at maximum 3.099%.

3.5 | The effectiveness of the aRCI on improving the voltage sag results comparison

The overall comparisons of the effectiveness of the simulated DER’s reactive power-based LVRT voltage support via aRCI on improving the voltage sag for all cases on both maxed aRCI and aRCI with K -factor 0.5 are shown in Table 10. Column ‘comparison A’ shows voltage sag improvement in scenario 2 in percentage as compared with voltage sag improvement in scenario 1 (aRCI with K -factor 0.5). Column ‘comparison B’ shows voltage sag improvement in scenario 3 (maxed aRCI) in percentage as compared with voltage sag improvement in scenario 1. It is observed that for higher X/R ratio cases, the DER’s LVRT voltage support via aRCI to minimise the voltage sag is more efficient.

TABLE 8 Comparison of maximum aRCI-enabled LVRT voltage control results between the proposed method and the Powerfactory DIgsilent simulations

Results	Method used	Case 1	Case 2	Case 3	Case 4	Case 5
$V_{DER_f} \angle \delta_{V_DER_f}$ ($p.u. \angle deg$)	DIgsilent	0.697 \angle -23.80	0.713 \angle -24.79	0.729 \angle -25.80	0.744 \angle -26.82	0.759 \angle -27.86
	Proposed method	0.719 \angle -1.82	0.739 \angle -1.68	0.739 \angle -1.53	0.761 \angle -1.39	0.769 \angle -1.25
$I_{dq_absolute_f}$ ($p.u.$)	DIgsilent	1.000	1.000	1.000	1.000	1.000
	Proposed method	1.000	1.000	1.000	1.000	1.000
$I_{d_ref_f}$ ($p.u.$)	DIgsilent	0.000	0.000	0.000	0.000	0.000
	Proposed method	0.000	0.000	0.000	0.000	0.000
$I_{q_ref_f}$ ($p.u.$)	DIgsilent	1.000	1.000	1.000	0.999	0.999
	Proposed method	1.000	1.000	1.000	1.000	1.000
$I_{P_DER_f}$ ($p.u.$)	DIgsilent	0.400	0.411	0.423	0.435	0.446
	Proposed method	0.128	0.116	0.104	0.092	0.081
$I_{Q_DER_f}$ ($p.u.$)	DIgsilent	0.916	0.911	0.906	0.901	0.895
	Proposed method	0.992	0.993	0.995	0.996	0.997

TABLE 9 % |Estimation difference| of maximum aRCI-enabled LVRT voltage control result

Results	V_{DER_f}	$\delta_{V_DER_f}$	$I_{dq_absolute_f}$	$I_{d_ref_f}$	$I_{q_ref_f}$	$I_{P_DER_f}$	$I_{Q_DER_f}$
Case 1	3.099	92.361	0	0	0	68.074	8.228
Case 2	3.647	93.239	0	0	0	71.883	8.986
Case 3	1.331	94.071	0	0	0.01	75.485	9.767
Case 4	2.231	94.835	0	0	0.1	78.808	9.551
Case 5	1.308	95.519	0	0	0.1	81.847	10.214

4 | ANALYSIS AND DISCUSSIONS

4.1 | Analysis

As can be seen, the voltage sag improvements predicted by the proposed method are reasonably close to the DIgsilent results, with the differences in the voltage sags estimation V_{DER_f} in all cases as indicated by the '% |estimation difference|' acceptably small. With the most considerable % |estimation difference| of the voltage sags estimation V_{DER_f} to be found at 3.64% in case 2 in the scenario of maximum aRCI-enabled LVRT, as shown in Table 9, the proposed method can estimate the effectiveness of aRCI at mitigating voltage sags effectively. The smallest % |estimation difference| of the voltage sags estimation V_{DER_f}

to be found at 1.3% in case 9 in the scenario of maximum aRCI-enabled LVRT is shown in Table 9 as well.

Further, the steady-state voltage rise estimated by the proposed method is relatively close to the DIgsilent results as well. The estimation difference of the steady-state voltage rise estimation V_{DER} of the proposed methodology in all cases as shown in Table 3 are observed most significant at only 0.123%, as shown in case 5, whereas the smallest estimation difference steady-state voltage rise estimation V_{DER} is found at 0.037% as shown in case 1.

Further, Table 10 shows that on the same level of reactive current injection, a lower voltage sag improvement can be observed on a lower X/R ratio system. This trend seems aligned with the argument that the DER connection to higher X/R ratio leads

TABLE 10 Voltage sag improvement of aRCI-enabled LVRT Voltage control system between the proposed and The DIgsilent methods in percentage

Results	Comparison A		Comparison B	
	Proposed method	DIgsilent method	Proposed method	DIgsilent method
Case 1	1.34	1.28	9.57	8.68
Case 2	2.14	1.6	11.71	10.4
Case 3	2.15	1.87	11.69	11.7
Case 4	2.11	1.98	13.84	13.53
Case 5	2.12	2.15	14.44	15.02

to more effective aRCI (better voltage sag improvement), which was claimed in many previous studies, such as in [10, 23]. It implies that the performance of the DER's LVRT voltage support via aRCI is highly dependent on the characteristic of the distribution grid (X/R ratio of the observed grid). Though in this study, X/R ratio variations are only set at the equivalent line impedance, $R_{line_tb} + jX_{line_tb}$, as shown in Table 1, and as explained in the first and the second steps of the proposed method, equivalent line impedance represents the 'collective impedance' of the observed grid in the form of a line between the external grid and the DER connection that is obtained from the impedance transformation process. Hence, one could imply that the equivalent line impedance $R_{line_tb} + jX_{line_tb}$ represents the X/R ratio of the observed grid.

The determination of the amount of the reactive current being injected is affected by the faulted voltage sag ΔV_{DER_f} (as implied in Equation 15 and thereby Equation 16). To estimate ΔV_{DER_f} , steady-state voltage rise magnitude $|V_{DER}|$ is needed. Thus, estimating $|V_{DER}|$ is essential since it is observed from Equation 14 that $|V_{DER}|$ determines the faulted voltage sag V_{DER_f} .

It has been shown that differences estimation between the proposed methodology and the Powerfactory DIgsilent method is observed on the reactive current injection $I_{Q_DER_f}$ (Table 7) and the active current injection $I_{P_DER_f}$ (Table 9). This is due to that in DIgsilent method, the voltage sag improvement that is estimated through dynamic RMS simulation requires θ' that is obtained from PLL. DIgsilent method considers the dynamic aspect of the simulation. In the proposed methodology, θ' is obtained from Equations (23) and (24). Equations (23) and (24) as suggested in [21] serve a similar function to the PLL. In the case of DIgsilent software, this is done via the time-domain RMS dynamic simulation; this transformation is available within the DER's inverter model, PLL, which is part of the DIgsilent model. The proposed methodology does not handle the dynamic aspects of the PLL's performance; however, it does not need to as its purpose is completely different. Further, note that the estimation of $\cos \theta'$ and $\sin \theta'$ that are obtained from Equations (23) and (24) rely on $V_{DER_f} \angle \delta_{V_DER_f}$. In the DIgsilent, $V_{DER_f} \angle \delta_{V_DER_f}$ is obtained based on each step of the derivation of all state variables during time-domain RMS dynamic simulation. This different way of interpreting $V_{DER_f} \angle \delta_{V_DER_f}$ and the way of obtaining θ' results in the estimation difference of $I_{P_DER_f}$ and $I_{Q_DER_f}$. Different results of θ' obtained by the proposed methodology and the DIgsilent method only causes the different interpretation of $\angle \delta_{V_DER_f} V_{DER_f}$. However, on estimating the effectiveness of aRCI, V_{DER_f} is the value that determines the voltage sag improvement. Thus, these different results can be ignored.

Aside from the matter as mentioned earlier, in most cases, the differences are small and acceptable as the proposed method does not account fully for the dynamic nature of the phenomenon simulated, unlike the DIgsilent simulation. Further, the proposed method can still be used reliably to estimate the voltage sag improvements.

4.2 | Discussions

The main feature of the proposed methodology is that it could estimate the effectiveness of aRCI on improving voltage sags without the need of the knowledge relating to the dynamic characteristic of the DER and way to construct the DER dynamic modelling. Thus, the methodology could avoid computational burden relating to the iterative process of the dynamic RMS simulation that is necessary to estimate the state derivatives of all state variables of the DER.

Though the verification of the proposed methodology does only account the balanced three-phase systems, the proposed methodology is still applicable on unbalanced three-phase systems, assuming all know the necessary information, such as negative-sequence component of the corresponding grid impedances, are obtainable.

Further, the proposed methodology can be used for aACI and aRACI applications. For aACI technique, this can be done by simply replacing Equations (15) to (17), (20), (26), and (27) with (29) to (34), respectively, and assuming K_{I_q} and ΔI_q in Figure 1 is replaced with K_{I_d} and ΔI_d , respectively.

$$\Delta I_{P_DER} = K_{I_d} \cdot \frac{|\Delta V_{DER_f} \angle \delta_{V_DER_f}| \mp V_{db}}{V_0 \angle \delta_0} \quad (29)$$

$$I_{P_DER} = I_{d_ref} = \begin{cases} I_{P_DER_prefault} + \Delta I_{P_DER}, & -I_{max} \leq I_{P_DER} \leq I_{max} \\ I_{max}, & -I_{max} > I_{P_DER} > I_{max} \end{cases} \quad (30)$$

$$I_{P_DER_prefault} = I_{DER_prefault} \cdot \sin(\varphi) \quad (31)$$

$$I_{Q_DER} = I_{q_ref} = I_{max} - |I_{P_DER}| \quad (32)$$

$$\begin{aligned} \Delta I_{DER_f} \angle \delta_{I_DER_f} &= (I_{DER_f} \angle \delta_{I_DER_f})_{K_{I_d}=n} - (I_{DER_f} \angle \delta_{I_DER_f})_{K_{I_d}=0} \\ &= (I_{DER_f} \angle \delta_{I_DER_f})_{K_{I_d}=n} - (I_{DER_f} \angle \delta_{I_DER_f})_{K_{I_d}=0} \end{aligned} \quad (33)$$

$$I_{f_aACI} \angle \delta_{I_f_aACI} = I_f \angle \delta_{I_f} + \Delta I_{DER_f} \angle \delta_{I_DER_f} \quad (34)$$

By applying the same sequence of the calculation, $\Delta I_{DER_f} \angle \delta_{I_DER_f}$ from Equation (33) represents the difference of DER's current contributions during a fault condition with and without the aACI. From Equation (33), the short-circuit current of the system with aACI-enabled DER, $I_{f_aACI} \angle \delta_{I_f_aACI}$ can be estimated with Equation (34). After $I_{f_aACI} \angle \delta_{I_f_aACI}$ has been found, Equations (12) to (14) are repeated with $I_f \angle \delta_{I_f}$ from Equation

(12), replaced by $I_{f_aACI} \angle \delta_{I_{f_aACI}}$. The improved voltage due to DER's aRCI is given as $V_{DER_f} \angle \delta_{V_{DER_f}}$ from Equation (14).

For aRACI technique, we can follow the procedure of the aRCI with some modification by replacing Equations (15) to (17), (20), (21), (26), and (27) with (35) to (39), respectively, assuming K_{I_q} and ΔI_q in Figure 1 is replaced with K_I and ΔI , respectively, and simply omitting Equations (17) to (20).

$$\Delta I_{DER} = K_I \cdot \frac{|\Delta V_{DER_f} \angle \delta_{V_{DER_f}}| \mp V_{db}}{V_0 \angle \delta_0} \quad (35)$$

$$I_{DER} = I_{ref} = \begin{cases} I_{DER_prefault} + \Delta I_{DER}, & -I_{max} \leq I_{DER} \leq I_{max} \\ I_{max}, & -I_{max} > I_{DER} > I_{max} \end{cases} \quad (36)$$

$$I_{DER} \angle \delta_{I_{DER}} = I_{DER} \angle \delta_{I_f} \quad (37)$$

$$\begin{aligned} \Delta I_{DER_f} \angle \delta_{I_{DER_f}} \\ = (I_{DER_f} \angle \delta_{I_f})_{K_I=n} - (I_{DER_f} \angle \delta_{I_{DER_f}})_{K_I=0} \end{aligned} \quad (38)$$

$$I_{f_aRACI} \angle \delta_{I_{f_aRACI}} = I_f \angle \delta_{I_f} + \Delta I_{DER_f} \angle \delta_{I_{DER_f}} \quad (39)$$

By doing the same process, $\Delta I_{DER_f} \angle \delta_{I_{DER_f}}$ from Equation (38) represents the difference of DER's current contributions during a fault condition with and without the aRACI. From Equation (38), the short-circuit current of the system with aRACI-enabled DER, $I_{f_aRACI} \angle \delta_{I_{f_aRACI}}$ can be estimated with Equation (39). After $I_{f_aRACI} \angle \delta_{I_{f_aRACI}}$ has been found, Equations (12) to (14) are repeated with $I_f \angle \delta_{I_f}$ from Equation (12), replaced by $I_{f_aRACI} \angle \delta_{I_{f_aRACI}}$. The improved voltage due to DER's aRACI is given as $V_{DER_f} \angle \delta_{V_{DER_f}}$ from Equation (14).

As mentioned earlier, other RPI techniques (RPI-Const-P, RPI-Const- I_d , and RPI-Const- $I_{g,max}$) are an alternative way to represent active and RPI techniques [7]. However, if we look further, these techniques are an extended variation of aRACI. It would be interesting to set up an exploratory study to cover these alternatives as a way to explore possible limitation of the proposed methodology if any.

The proposed methodology indeed does not consider noise and signals attenuation in the distribution network. This can be understood since the methodology does not handle and therefore not cover the dynamic aspects in the study. However, LVRT is a millisecond phenomenon, whereas its frequency range is classified as transient recovery voltage; and it is around 50/60 Hz–20 kHz for terminal fault and 50/60 Hz–100 kHz for short-line fault [24]. Since the methodology is meant for estimating the effectiveness of aRCI on improving voltage sags, the method is made to capture the fast-transient response of the DER upon voltage sag. With that in mind, it can be assured distribution network noise, such as switching noise from commer-

cial component will not affect the estimations and hence affect the performance of the resulted voltage sag improvement.

Therefore with such feature in the proposed methodology, one could understand clearer 'the flow', the whole process of estimating the effectiveness of aRCI on improving voltage sags, from the process of the voltage sags to the evaluation of the voltage sags improvement on the aRCI-enabled DER-connected bus. Furthermore, from a practical viewpoint, the proposed methodology can support distribution system operators or a DER grid planner in the event they need to justify practical grid support requirements for fault ride-through on a particular distribution network.

5 | CONCLUSION

5.1 | Summary

Methodology for estimating the effectiveness of DER's voltage control via aRCI for LVRT support is given. As explained in the introduction, without the need to perform a computation process that inherently has iterative nature (computing derivatives of all state variables of the DER to estimate the dynamic response of the DER), the proposed methodology still could successfully estimate the effectiveness of aRCI in improving voltage sags. Further, one could take benefit from the proposed methodology on a grid planning to estimate the effectiveness of the DER's LVRT voltage support via aRCI without the need to concern if the grid information is incomplete—information that is often needed on dynamic RMS-based simulation; for example, a commercial software tool such as DIgSilent PowerFactory.

5.2 | Recommendations

From the research work, a suggested approach for grid planning upon implementing aRCI-based LVRT voltage support is presented.

Upon implementing aRCI-based LVRT voltage support, it is best to understand to the topology of the distribution grid, the information required to construct the implementation, and the information available to support the planning. In the event that some information is unobtainable or too cumbersome/challenging to estimate, such as the aggregated dynamic characteristic of the DER, the mixture of the load, and the exact profile of the active and reactive power of both from the DER and the distribution loads, then estimating the effectiveness of the aRCI-based LVRT voltage support through the proposed methodology can be a useful and practical option. Through simplifications and reasonable assumptions, such as averaging the active and reactive power of the distribution loads, then aggregating the known impedance of the distribution line, and assuming the likeliest located voltage sag, the effectiveness of the support in minimising voltage sag could be estimated. The obtained result could be then used to judge the necessity of the implementation of the support.

ORCID

Akbar Swandaru  <https://orcid.org/0000-0001-7262-9471>
 Jan K. Sykulski  <https://orcid.org/0000-0001-6392-126X>

REFERENCES

- Göksu, Ö.: Control of Wind Turbines during Symmetrical and Asymmetrical Grid Faults. Aalborg University, Department of Energy Technology, Aalborg, (2012)
- Weise, B.: Impact of K-factor and active current reduction during fault-ride-through of generating units connected via voltage-sourced converters on power system stability. *IET Renewable Power Gener.* 9(1), 25–36 (2015)
- Erlich, I., Shewarega, F., Engelhardt, S.: Effect of wind turbine output current during faults on grid voltage and the transient stability of wind parks. Paper presented at the 2009 IEEE power energy society general meeting, Calgary, AB, Canada, 26–30 July 2009 <https://doi.org/10.1109/PES.2009.5275626>
- Bae, Y., Vu, T.K., Kim, R.Y.: Implemental control strategy for grid stabilization of grid-connected PV system based on German grid code in symmetrical low-to-medium voltage network. *IEEE Trans. Energy Convers.* 28(3), 619–631 (2013)
- Complete Grid Code: National UK Grid Code. In: Grid Code Panel Meeting, Gallows Hill, Warwick, UK (2020)
- Miret, J., Camacho, A., Castilla, M.: Reactive current injection protocol for low-power rating distributed generation sources under voltage sags. *IET Power Electron.* 8(6), 879–886 (2015)
- Brandao, D.I., Mendes, F.E.G., Ferreira, R.V.: Active and reactive power injection strategies for three-phase four-wire inverters during symmetrical/asymmetrical voltage sags. *IEEE Trans. Ind. Appl.* 55(3), 2347–2355 (2019)
- Kayikci, M., Milanovic, J.V.: Reactive power control strategies for DFIG-based plants. *IEEE Trans. Energy Convers.* 22(2), 389–396 (2007)
- Martínez, J., Kjær, P.C., Rodríguez, P.: Active current control in wind power plants during grid faults. *Wind Energy* 13(8), 737–749 (2010)
- Boemer, J.: On stability of sustainable power systems: Network fault response of transmission systems with very high penetration of distributed generation <https://repository.tudelft.nl/islandora/object/uuid%3A78bffb19-01ed-48f9-baf6-ffb395be68a0> (2016) <https://doi.org/10.4233/uuid:78bffb19-01ed-48f9-baf6-ffb395be68a0>
- Goksu, O., Teodorescu, R., Bak, C.L.: Instability of wind turbine converters during current injection to low voltage grid faults and PLL frequency based stability solution. *IEEE Trans. Power Syst.* 29(4), 1683–1691 (2014)
- Heinrich, C., Fortenbacher, P., Fuchs, A.: PV-integration strategies for low voltage networks. In: 2016 IEEE International Energy Conference (ENERGYCON), Leuven, Belgium, (2016)
- Awadhi, N.A., Moursi, M.S.E.: A novel centralized PV power plant controller for reducing the voltage unbalance factor at transmission level interconnection. *IEEE Trans. Energy Convers.* 32(1), 233–243 (2017)
- Lammert, G. et al.: Impact of fault ride-through and dynamic reactive power support of photovoltaic systems on short-term voltage stability. In: 2017 IEEE Manchester PowerTech, Manchester, UK. (2017)
- Mishra, A., Nair, N.K.C., Patel, N.D.: Fault current characterisation of single phase inverter systems. In: 2017 IEEE Power Energy Society General Meeting, Chicago, IL, USA (2017)
- Roediger, S., Yan, R., Saha, T.K.: Investigation of the impacts of three-phase photovoltaic systems on three-phase unbalanced networks. In: 2012 IEEE Power and Energy Society General Meeting, San Diego, CA, USA (2012) <https://doi.org/10.1109/PESGM.2012.6344697>
- IEC 60909-0: Short-circuit currents in three-phase AC systems—Part 0: Calculation of currents, 1st edition. IEC, London, (2000–2007)
- IEC 60909-0: Short-circuit currents in three-phase AC systems –Part 4: Examples for the calculation of short-circuit currents. 1st edition. IEC, London (2001–2007)
- Elrayment, A.Y., Wanik, M.Z.C., Bousseham, A.: Simplified approach to analyze voltage rise in LV systems with PV installations using equivalent power systems diagrams. *IEEE Trans. Power Delivery* 32(99), 2140–2149 (2016)
- Samadi, A., Soder, L., Shayesteh, E.: Static equivalent of distribution grids with high penetration of PV systems. *IEEE Trans. Smart Grid.* 6(4), 1763–1774 (2015)
- Teodorescu, R., Liserre, M., Rodriguez, P.: Grid converters for photovoltaic and wind power systems. Wiley, Chichester, West Sussex (2011)
- Wu, J., He, Y., Jenkins, N.: A robust state estimator for medium voltage distribution networks. *IEEE Trans. Power Syst.* 28(2), 1008–1016 (2013)
- Camacho, A., Castilla, M., Miret, J.: Reactive power control for distributed generation power plants to comply with voltage limits during grid faults. *IEEE Trans. Power Electron.* 29(11), 6224–6234 (2014)
- Das, J.C.: Transients in Electrical Systems. McGraw-Hill Professional Publishing, New York, USA (2010)

How to cite this article: Swandaru A, Rotaru MD, Sykulski JK. A simple method for estimating the effectiveness of reactive power-based low-voltage ride-through support of the distributed energy resources. *IET Renew Power Gener.* 2021;15:1149–1162. <https://doi.org/10.1049/rpg2.12095>